Comparative Medicine
Copyright 2015
by the American Association for Laboratory Animal Science

Vol 65, No 6
December 2015
Pages 517–525

Original Research

Temporal Evolution of MRI Characteristics in Dogs with Collagenase-Induced Intracerebral Hemorrhage

Daegi An,[1,2] Junyong Park,[3] Jong-Il Shin,[4] Hyung-Joong Kim,[5] Dong-In Jung,[6] Ji-Houn Kang,[2] Gonhyung Kim,[2] Dong-Woo Chang,[2] Jung-Hyang Sur,[4] Mhan-Pyo Yang,[2] Chulhyun Lee,[3,†] and Byeong-Teck Kang[1,2,†*]

Intracerebral hemorrhage (ICH) is one of the most lethal types of stroke. Neuroimaging techniques, particularly MRI, have improved the diagnostic accuracy of ICH. The MRI characteristics of the evolving stages of ICH in humans—but not those in dogs—have been described. In this study, we document the temporal MRI characteristics in a canine model of collagenase-induced ICH. Specifically, ICH was induced in 5 healthy beagles by injecting 500 U of bacterial collagenase from *Clostridium histolyticum*, which was delivered into the parietal lobe over 5 min by using a microinfusion pump. T1- and T2-weighted, fluid-attenuated inversion recovery, gradient-echo (GRE), and diffusion-weighted (DWI) imaging and measurement of the apparent diffusion coefficient (ADC) were performed serially at 6 different time points (before and 12 h, 3 d, 5 d, 10 d and 24 d after hemorrhage) by using a 3-T MR system. The temporal changes of T1 signal intensity (SI) corresponded well with the reported human data. The temporal changes of T2 and GRE sequences, with the exception of T2 and GRE hyperintensities at the early subacute stage, also matched. ADC measurements were high at the early subacute stage, and DWI-SI positively correlated with T2- and GRE-SI from the early subacute stage onward. In conclusion, MRI is an ideal method for characterizing the temporal evolution of parenchymal alterations after ICH in dogs. These data might be useful for differentiating clinical stages of ICH in dogs.

Abbreviations: ADC, apparent diffusion coefficient; DWI, diffusion-weighted imaging; FLAIR, fluid attenuation inversion recovery; GRE, gradient echo; ICH, intracerebral hemorrhage; ROI, region of interest; SIR, signal intensity ratio; WI, weighted imaging

Intracerebral hemorrhage (ICH) occurs in 15% to 20% of all stroke patients.[10] In comparison with ischemic stroke, patients with ICH are at higher risk of death and long-term functional disability.[10] Most survivors remain disabled, owing to the hematoma within the brain parenchyma, which can cause severe neurologic deficits.

Because of the rapid progression of brain damage during the first hours after ICH, quick recognition and diagnosis are key. Clinical signs are helpful for early diagnosis but are insufficient for the differentiation of ICH from other stroke subtypes. Brain imaging techniques, including CT and MRI, have helped improve the accuracy of diagnosis, which is necessary for the appropriate treatment of acute cerebrovascular accidents.[5] Previously, MRI was considered unsuitable for detecting early-stage hemorrhage. However, MRI recently was shown to have high sensitivity for detecting hyperacute ICH, superior even to CT.[21] MRI is now considered the ideal imaging modality for characterizing the temporal and spatial evolution of parenchymal changes after ICH.[30]

The MRI characteristics of ICH vary with the duration of the hematoma, the type of MRI sequence, and various biologic factors.[17] The several forms of hemoglobin (oxyhemoglobin, deoxyhemoglobin, and methemoglobin), which have different magnetic properties, are observed at different times points during hemorrhage, depending on whether they contain unpaired electrons.[28] The MR signal intensity (SI) of hemorrhage has been reported for various animal models, from in vitro studies, and during clinical observations.[2,6,12,24] Reflecting the breakdown products of hemoglobin, the MRI features of 5 distinctive stages of ICH have been reported in humans: hyperacute (within 24 h of hemorrhage; intracellular oxyhemoglobin; long T1 and T2 values; iso- to hypointense on T1-weighted images [WI], hyperintense on T2WI); acute (1 to 3 d; intracellular deoxyhemoglobin; long T1, short T2 values; hypointense on T1WI, hypointense on T2WI); early subacute (3 to 7 d; intracellular methemoglobin with intact erythrocyte; short T1 and T2 values; hyperintense on T1WI, hypointense on T2WI); late subacute (7 to 14 d; extracellular methemoglobin with erythrocyte lysis; short T1, long T2 values; hyperintense on T1WI and T2WI); and chronic (after 14 d; ferritin and hemosiderin; long T1, short T2 values; hypointense on T1WI and T2WI).[4]

Received: 28 Feb 2015. Revision requested: 16 Jun 2015. Accepted: 28 Jun 2015.
[1]Laboratory of Molecular Imaging and Translational Research and [2]Veterinary Medical Center, College of Veterinary Medicine, Chungbuk National University, Cheongju, South Korea; [3]Division of Convergence Biotechnology, Korea Basic Science Institute, Ochang, South Korea; [4]Department of Veterinary Pathology, Small Animal Tumor Diagnostic Center, College of Veterinary Medicine, Konkuk University, Seoul, South Korea; [5]Department of Biomedical Engineering, Kyung Hee University, Yongin, South Korea; and [6]Research Institute of Life Sciences, Gyeongsang National University, Jinju, South Korea

[†]These authors contributed equally to this work

**Corresponding author. Email: kangbt@chungbuk.ac.kr*

So far, very few clinical studies have assessed the time-dependent evaluation of MRI patterns beyond 24 h in dogs.[23] The clinical setting presents several difficulties to the study of ICH. Because ICH patients are often critically ill, requiring physiologic support, most patients with ICH are unsuitable for MRI due to their medical instability.[15] In dogs, it is frequently impossible to ascertain the precise interval between hemorrhage and MRI scanning. An animal model offers several advantages for studying ICH: histologic analysis in survivors of ICH, the initial testing of novel interventions, homogeneous experimental groups, and a predictable onset of ICH.[27]

An experimental animal model used in human medicine should exhibit certain characteristics, such as ease of standardization and reproducibility, and representation of the principal mechanisms associated with the particular condition in humans.[8] Small-animal (for example, mice, rats, gerbils) and large-animal (for example, cats, dogs, pigs, sheep, monkeys) models that demonstrate these characteristics have been developed. Although small animals are often more cost-effective and allow for relatively simpler genetic manipulation and management, the use of large-animal models is important in preclinical studies of ICH because these animals have gyrencephalic brains with well-developed white matter that are structurally and functionally similar to human brains.[16] Notably, numerous experimental treatment strategies have been evaluated successfully in rodent models and in vitro, but the vast majority of such modalities subsequently have failed in clinical trials.[18] For all of these reasons, the Stroke Therapy Academic Industry Roundtable strongly recommends the use of appropriate large-animal models of stroke.[19] Among large animals, dogs are readily and economically available, easy to care for, and have predictable intercurrent diseases.

Presently, MRI of the brain is extremely useful in confirming stroke, determining the extent of the lesion, and distinguishing between ischemic and hemorrhagic stroke. However, MRI findings of canine ICH are largely based on results from human studies, given the paucity of relevant canine studies. A previous study demonstrated that the time course of ICH stages is much faster in rats than in humans.[3] Therefore, we hypothesized that the temporal MRI characteristics of evolving stages of canine ICH differ from those of ICH in humans.

Advanced MRI techniques may enable clarification of mechanisms that mediate injury after ICH. Diffusion-weighted imaging (DWI) has already proven useful in the diagnosis and investigation of the natural history of ischemic stroke.[7] However, the usefulness of those techniques to assess mechanisms of neuronal injury after ICH remains a topic of debate, both in humans and in dogs. Therefore, the purpose of the current study was to evaluate the utility of advanced MRI techniques, including DWI, in the diagnosis of canine ICH, by monitoring the temporal changes in MR images relative to the stage of hematoma in affected dogs.

Materials and Methods

Animals and ethical statements. This study population comprised 5 healthy laboratory beagles (3 male and 2 female; age, 3 to 5 y; weight, 12 to 14 kg; Harlan Interfauna, Huntingdon, Cambridgeshire, UK). None of the dogs had signs of neurologic problems on physical examination. They were screened for metabolic disease by means of CBC and serum chemistry analysis and acclimated to the facility for a minimum of 1 wk prior to being used in the present study. The dogs were housed individually and fed twice daily with a commercial dry food (Science Diet, Hill's Pet Nutrition, Topeka, KS). Fresh water was supplied continuously by an automatic dispenser at our well-ventilated facility under controlled light–dark cycles (light on, 0800 to 2000). An indoor temperature range of 18 to 24 °C and a humidity level of 55% ± 10% with 8 air changes hourly were maintained. The experiment was approved by the IACUC (CBNUA-591-13-01) of the Laboratory Animal Research Center of Chungbuk National University. The approved study endpoint was 24 d after the induction of ICH. After completion of the imaging studies at 24 d after the induction of hemorrhage, all dogs were euthanized with sodium pentobarbital (80 mg/kg IV; Entobar Injection, Hanrim Pharm, Gyeonggi, South Korea).

Animal preparation, monitoring, and surgical procedure. Dogs were fasted for 12 h before the induction of propofol (5 mg/kg IV; Provive, Myungmoon Pharm, Seoul, South Korea) anesthesia, oral intubation, and mechanical ventilation. Anesthesia was maintained with isoflurane (Terrell; Piramal Healthcare, Bethlehem, PA) at 2% to 3% of the inspired volume during surgery in a rebreathing circle system. The oxygen delivery and ventilation rates were monitored continuously and adjusted as needed to maintain heart rate and blood oxygen saturation within normal limits. Rectal temperature was monitored continuously and kept at 37 to 38 °C by using a thermostatically controlled heating pad (Gaymar Industries, Orchard Park, NY).

The dogs were placed in a stereotactic apparatus (model 1504, David Kopf Instruments, Tujunga, CA), and a burr hole was created. A 20-gauge needle (BD PrecisionGlide; Becton Dickinson Medical, Singapore, Singapore) was implanted into the right parietal lobe. ICH was induced by injecting 500 U of bacterial collagenase from *Clostridium histolyticum* (type XI, Sigma Chemical, St Louis, MO) in 50 µL of sterile saline and 50 µL of heparin (20,000 U/mL). The solution was delivered over 5 min by using a microinfusion pump (KDS 100; KD Scientific, Holliston, MA). After an additional 5 min, the needle was removed slowly to avoid backflow. The hole was sealed with bone wax (AnyTemp NE; Mdclus, Cheongju, South Korea), and the incision site was sutured.

Postsurgical management. After surgery, the dogs were awakened from anesthesia and then returned to the cages in the animal recovery room. A recirculating warm-water blanket was placed beneath a portion of each cage. The dogs were observed continuously until they had fully recovered (approximately 8 h). The next day, the dogs were transported to the holding area and monitored periodically until euthanasia. Ampicillin (20 mg/kg PO every 12 h; Ampi10, UniBiotech, Chungchongnam-Do, South Korea) was administered to the dogs for 1 wk to prevent bacterial infection. The incision site was examined and cleaned on follow-up until healed. To control pain, butorphanol (0.4 mg/kg IM; Butophan, Myungmoon Pharm, Seoul, South Korea) was given as needed, usually twice daily for the first 3 to 5 d after surgery.

Neurologic evaluation. Neurologic deficits were assessed at several time points (12 h and 3, 5, 10, and 24 d after surgery) as described previously.[14] An experienced observer performed scored motor function (1, no deficit; 2, hemiparetic but able to walk; 3, stands only with assistance; 4, hemiplegic and unable to stand; 5, comatose or dead, cannot be determined), consciousness (1, normal; 2, mildly reduced; 3, severely reduced; 4, comatose or dead), head turning (0, absent; 1, posturing and turns toward the side of the hematoma; 2, unable to lift head, comatose, or dead),

Table 1. Summary of scan parameters

Parameters	T1	T2	FLAIR	GRE	DWI
Repetition time (ms)	500	4000	10000	677	4164
Echo time (ms)	20	80	125	16	107
Flip angle (degrees)	90	90	90	18	90
Number of slices	28	28	28	28	28
Slice thickness (mm)	3	3	3	3	3
Interslice gap (mm)	0	0	0	0	0
Number of averages	1	2	2	2	2
Field of view (mm)	130 × 130	130 × 130	130 × 130	130 × 130	150 × 150
Acquisition matrix	304 × 250	304 × 294	304 × 220	304 × 356	140 × 140
Measured voxel size (mm)	0.43 × 0.52	0.43 × 0.43	0.43 × 0.51	0.43 × 0.37	1.10 × 1.08
Acquisition time (min:s)	4:14	5:52	7:00	8:05	1:28

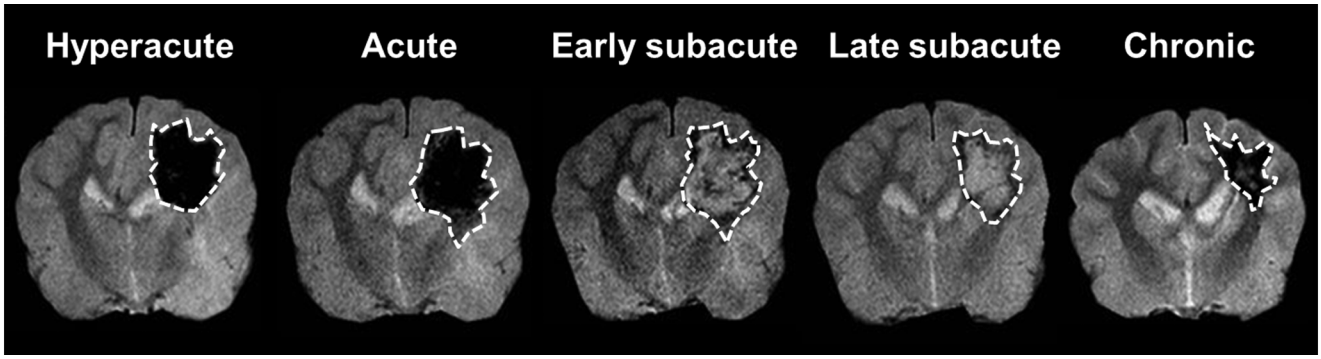

Figure 1. Representative GRE images showing the ROI (dotted lines) placed on hemorrhagic lesions at different stages of ICH.

Table 2. Neurologic scores (mean ± 1 SD) of 5 dogs after hematoma induction

	12 h	3 d	5 d	10 d	24 d
Motor function	1.00 ± 0	1.00 ± 0	1.00 ± 0	1.00 ± 0	1.00 ± 0
Consciousness	1.60 ± 0.55	1.00 ± 0	1.00 ± 0	1.00 ± 0	1.00 ± 0
Head turning	0.40 ± 0.55	0 ± 0	0 ± 0	0 ± 0	0 ± 0
Circling	0 ± 0	0 ± 0	0 ± 0	0 ± 0	0 ± 0
Hemianopsia	0 ± 0	0 ± 0	0 ± 0	0 ± 0	0 ± 0
Overall	3.00 ± 1.00	2.00 ± 0	2.00 ± 0	2.00 ± 0	2.00 ± 0

circling (0, absent; 1, present; 2, unable to walk, or dead), and hemianopsia (0, absent; 1, present; 2, unable to test because of reduced consciousness or death). According to this scoring system, a completely normal dog would have a total score of 2, whereas a dog with the most severe deficits (comatose or dead) would have a total score of 15.

Imaging protocol. The MRI examinations were performed by using a 3-T MR system (Achieva 3.0 TTX, Philips Medical System, Best, The Netherlands). The scans were performed serially at 6 time points: before (baseline) and 12 h (hyperacute), 3 d (acute), 5 d (early subacute), 10 d (late subacute), and 24 d (chronic) after induction of ICH. All images were acquired with the dogs in sternal recumbency under general anesthesia, which was induced with medetomidine (20 µg/kg IM; Domitor, Pfizer, Seoul, South Korea) and maintained with tiletamine–zolazepam (8 mg/kg IV; Zoletil, Virvac, Carros, France). The MRI protocol included T1WI, T2WI, fluid-attenuated inversion recovery (FLAIR) sequences, gradient-echo (GRE) sequences, and DWI and measurement of the apparent diffusion coefficient (ADC; Table 1).

Image analysis. MIPAV software (Biomedical Imaging Research Services Section, National Institutes of Health, Bethesda, MD) was used to trace hemorrhagic lesions (hypo- or hyperintense areas) on GRE images. For quantitative analysis, regions of interest (ROI) were placed on determined hemorrhagic lesions with different SI, for comparison with normal contralateral regions at each time point (12 h and 3, 5, 10, and 24 d after surgery; Figure 1). In addition, from the GRE images obtained before surgery, ROI outlining the right side of the parietal lobes were created because of the absence of hematoma. Established ROI were moved to the corresponding area of other MRI images (T1, T2, FLAIR, DWI, and ADC), and then SI was measured in each ROI and in homologous regions of the contralesional hemisphere. The SI ratio (SIR) was obtained by normalizing the SI of the hemorrhagic lesion to the SI of the corresponding contralateral region. Statistical

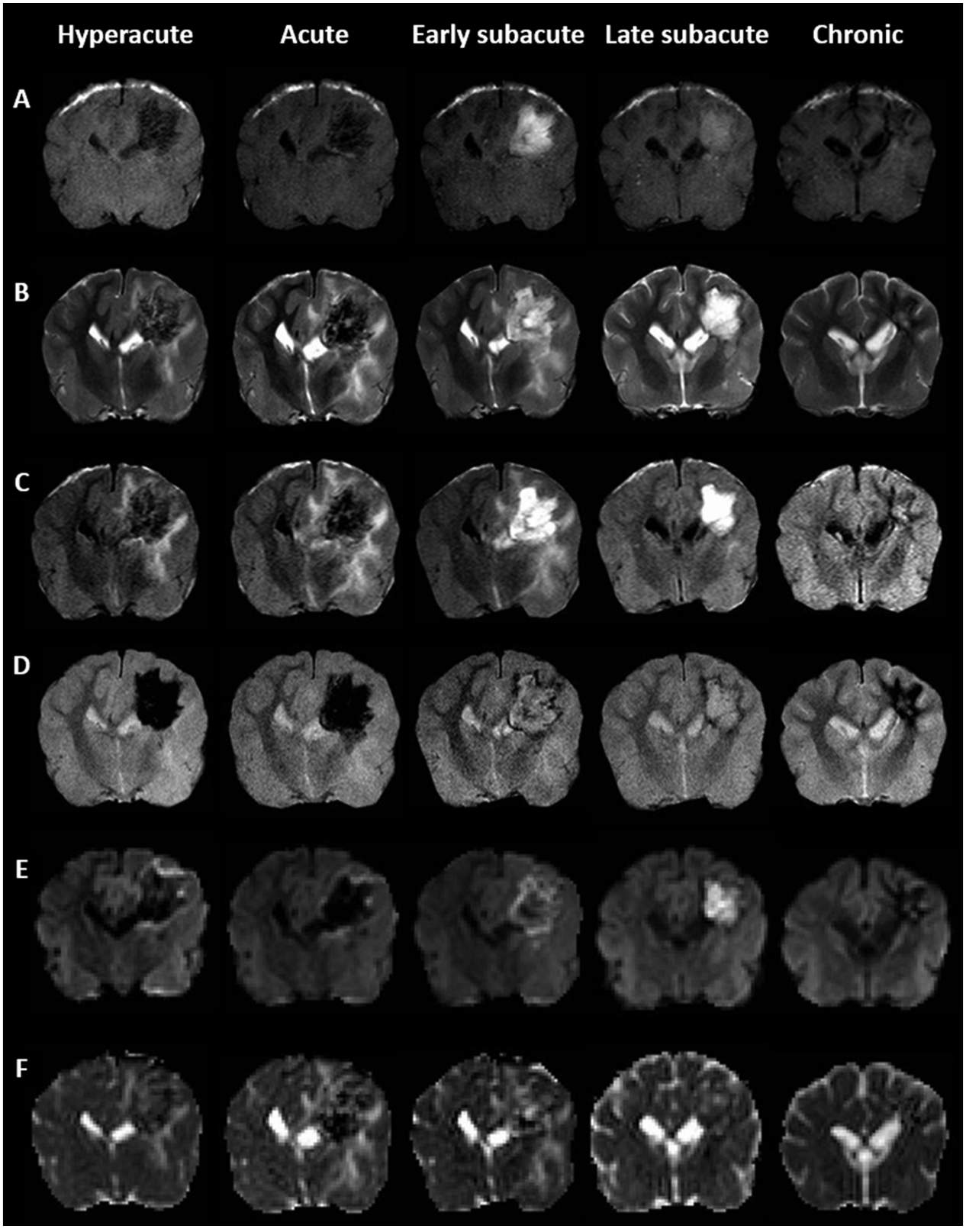

Figure 2. Representative (A) T1WI, (B) T2WI, (C) FLAIR, (D) GRE, (E) DWI, and (F) ADC maps illustrating the temporal evolution of hemorrhagic lesions according to the evolving stages. Hematomas in the right side of the parietal lobe underwent rapid and reversible changes in signal intensity, which varied with the pulse sequence.

Table 3. MRI characteristics of hematomas according to the evolving stages

	T1	T2	FLAIR	GRE	DWI	ADC
Hyperacute	hypointensity	hypointensity and hyperintensity	hypointensity and hyperintensity	hypointensity	hypointensity	hypointensity, isointensity, and hyperintensity
Acute	hypointensity	hypointensity and hyperintensity	hypointensity and hyperintensity	hypointensity	hypointensity	hypointensity, isointensity, and hyperintensity
Early subacute	hyperintensity	hyperintensity	hyperintensity	hyperintensity	hyperintensity	hyperintensity
Late subacute	hyperintensity	hyperintensity	hyperintensity	hyperintensity	hyperintensity	hypointensity, isointensity, and hyperintensity
Chronic	hypointensity to isointensity	hypointensity	hypointensity and hyperintensity	hypointensity	hypointensity	hypointensity

comparison of the SIR obtained before and after surgery ensured that the MRI characteristics of hematoma were graded objectively as hyper- and hypointensity at each stage: hyperintensity was defined as a significant increase of the SIR compared with the value obtained before surgery, whereas hypointensity was a significant decrease of the SIR. When objective analysis did not reveal a significant difference between the SIR before and after surgery, MR images were reviewed subjectively, and the hemorrhagic lesions were graded as hyper-, iso-, and hypointense. For quantitative measurements of the evolution of vasogenic and cytotoxic edema, T2 and ADC values were measured from created ROI overlaid onto corresponding T2 and ADC maps.

The hemorrhagic areas determined on the GRE images were multiplied by the section thickness and summed to produce the total hematoma volume.

Histopathology. After imaging studies were completed, the brains were removed and dissected into coronal 2-mm sections. Brain slices were placed in 10% paraformaldehyde in PBS. Transverse sections (4 µm) of paraffin-embedded tissue were used for hematoxylin and eosin staining to assess neuronal damage and macrophage infiltration. Macrophages were identified by their morphologic features, including ovoid or indented nucleus and abundant cytoplasm with numerous small vacuoles. Macrophages were counted at 3 hemorrhagic sites under 400× magnification, and an average was taken as the absolute macrophage count. Prussian blue staining was used to demonstrate ferric iron in tissue sections.

Statistical analysis. Data are presented as mean ± 1 SD. One-way repeated-measures ANOVA with the Bonferroni posthoc test was used to evaluate sequential changes of the SIR, T2, and ADC values of hematomas. Pearson correlation was used to investigate the relationship between the SIR of hemorrhagic lesions on DWI and those estimated on T2, GRE, and ADC images. Statistical significance was set as a P value less than 0.05. Statistical analysis was performed by using the SPSS package (version 12.0; IBM, Chicago, IL).

Results

All 5 dogs survived the surgical procedure and participated in all measurements performed before and after surgery. Hematomas were induced in the right side of the parietal lobe after injection of bacterial collagenase, but there were no physiologic and neurobehavioral abnormalities except for mildly reduced consciousness (3 dogs) and head turning (2 dogs) at 12 h after surgery. These neurologic deficits disappeared by 3 d after hematoma induction (Table 2). (Figure 2) shows representative T1WI, T2WI, FLAIR, GRE, DWI, and ADC maps, to illustrate the temporal evolution of hemorrhagic lesions.

Image analysis. The MRI characteristics of the induced hemorrhagic lesions are summarized in (Table 3).

T1WI. Hemorrhagic lesions on T1WI were apparent as hypointensities during the hyperacute and acute stages, hyperintensities at the early and late subacute stages, and mixed intensities (hypo- to isointensity) at the chronic stage (Figure 2 A). Compared with that at baseline, the SIR of hemorrhagic lesions were significantly decreased at the hyperacute (that is, 12 h; $P < 0.01$) and acute (day 3, $P < 0.05$) stages, whereas they were significantly increased at the early (day 10, $P < 0.01$) and late (day 24, $P < 0.05$) subacute stages (Figure 3 A).

T2WI and FLAIR images. Hemorrhagic lesions at early and late subacute stage were characteristically hyperintense on both T2 (Figure 2 B) and FLAIR (Figure 2 C) images. In contrast, hyperacute, acute, and chronic hemotomas had mixed intensities (hypo- and hyperintensity; Figure 2 B and C). The T2 and FLAIR SIR were increased at early subacute stage (baseline compared with day 5, $P < 0.01$ for both comparisons), whereas decreased SIR was present on T2WI during the chronic stage only (day 24, $P < 0.05$; Figure 3 B and C).

GRE imaging. GRE scanning revealed hypointensities in hematomas at the hyperacute, acute, and chronic stages but hyperintensities at the early and late subacute stages (Figure 2 D). The GRE SIR were significantly decreased at hyperacute, acute, and chronic stage (baseline compared with 12 h, day 3, and day 24, respectively; $P < 0.01$ for all comparisons). However, the changes in the SIR at early and late subacute stages did not reach statistical significance (Figure 3 D).

DWI. Hyperacute, acute, and chronic hematomas were hypointense on DWI, whereas early and late subacute hematomas were hyperintense (Figure 2 E). Measurement of DWI SIR yielded an increased value at the early subacute stage (baseline compared

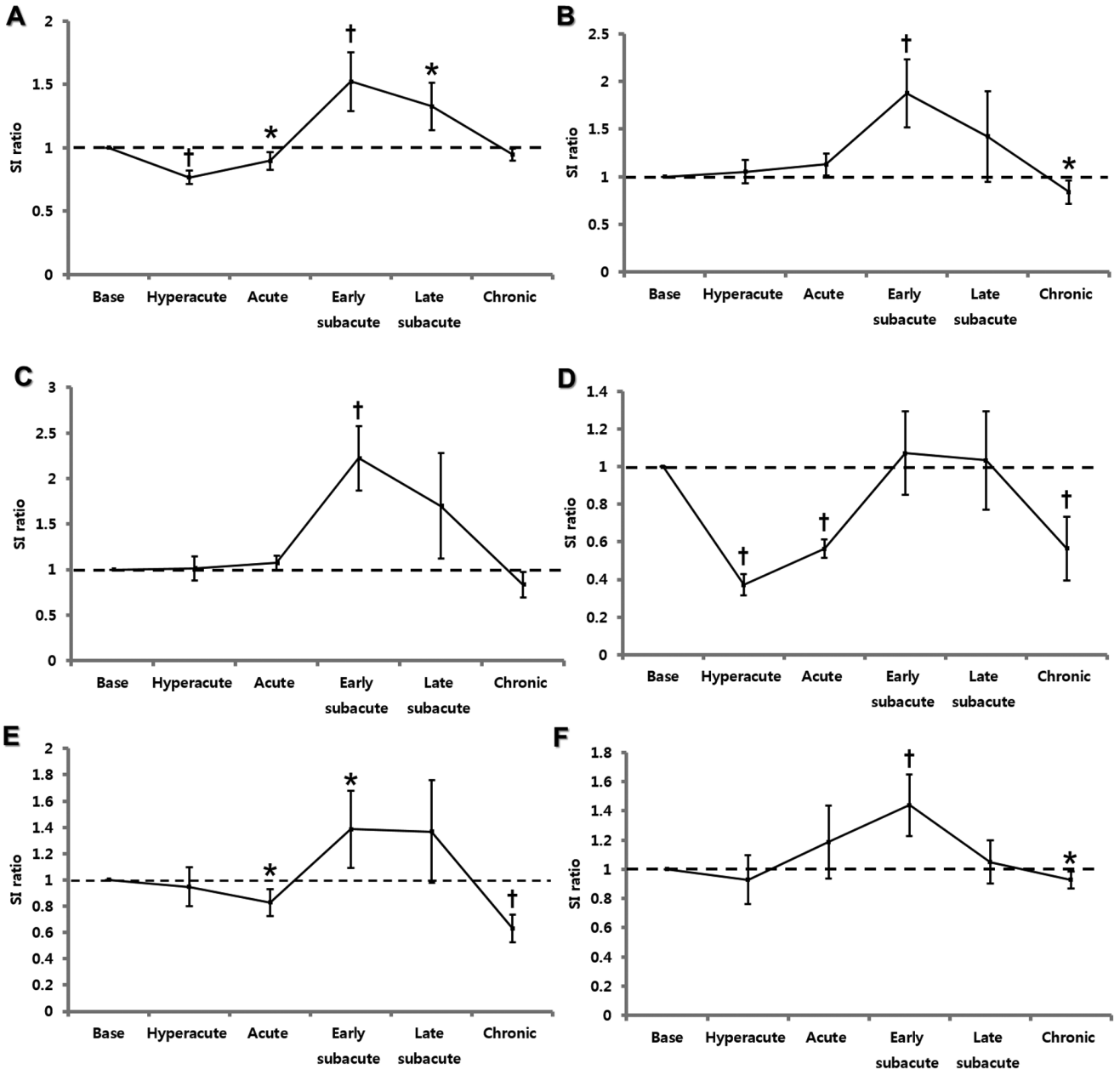

Figure 3. Temporal evolution of the SIR measured from (A) T1WI, (B) T2WI, (C) FLAIR, (D) GRE, (E) DWI, and (F) ADC maps according to the evolving stages. Value significantly (*, $P < 0.05$; †, $P < 0.01$; one-way repeated-measures ANOVA with Bonferroni posthoc test) different from baseline SIR.

with day 5, $P < 0.05$) but decreased values at the acute (day 3, $P < 0.05$) and chronic (day 24, $P < 0.01$) stages (Figure 3 E).

ADC mapping. Most hemorrhagic lesions on ADC maps were mixed in intensity (hypo-, iso-, and hyperintense), except for hyperintensity at the early subacute stage (Figure 2 F). The ADC SIR were increased at early subacute stage (baseline compared with day 5, $P < 0.01$) and decreased at chronic stage (day 24, $P < 0.05$; Figure 3 F).

Correlations between DWI SIR and T2, GRE, and ADC SIR. The correlations between the DWI SIR and T2, GRE, and ADC SIR of hemorrhagic lesions are shown in (Table 4). The DWI SIR was positively correlated with the T2 and GRE SIR at the early subacute (day 5, $r = 0.97$ [$P < 0.01$] and $r = 0.99$ [$P < 0.01$], respectively), late subacute (day 10, $r = 0.95$ [$P < 0.05$] and $r = 0.89$ [$P < 0.05$], respectively), and chronic (day 24, $r = 0.92$ [$P < 0.05$] and $r = 0.91$ [$P < 0.05$], respectively) stages. However, the DWI and ADC SIR were not correlated significantly at any measurement time.

Measurements of T2 and ADC values. Similar to the change in SIR, T2 values were increased at early subacute stage (day 5, $P < 0.05$; Figure 4 A), whereas increased ADC values were present at both the early subacute and chronic stages (days 5 and 24, $P < 0.05$ for both comparisons; Figure 4 B).

Hematoma volume. The largest mean hematoma volume on the GRE images occurred at 3 d after surgery and gradually decreased thereafter until the end of study period (Table 5).

Table 4. Correlations between DWI-SIR and T2-, GRE-, and ADC-SIR of hemorrhagic lesions

	Hyperacute		Acute		Early subacute		Late subacute		Chronic	
	r	*P*	*r*	*P*	*r*	*P*	*r*	*P*	*r*	*P*
DWI-T2	0.54	0.35	0.44	0.45	0.97	0.006	0.95	0.02	0.92	0.03
DWI-GRE	0.25	0.69	0.37	0.54	0.99	0.002	0.89	0.04	0.91	0.03
DWI-ADC	−0.43	0.47	−0.35	0.57	−0.23	0.97	0.69	0.20	0.75	0.14

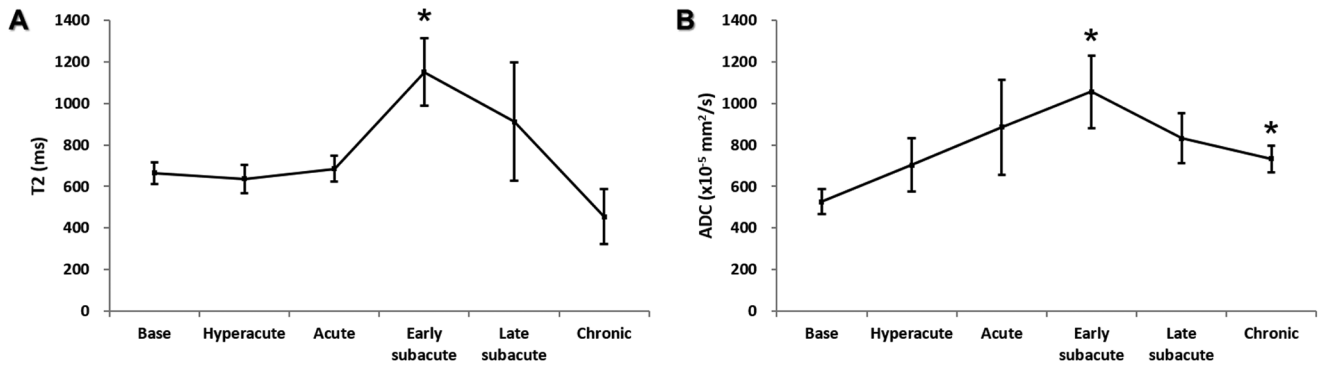

Figure 4. Temporal evolution of T2 and ADC values measured from corresponding (A) T2 and (B) ADC maps according to the evolving stages. *, Value significantly ($P < 0.05$; one-way repeated measures ANOVA with Bonferroni posthoc test) different from baseline.

Table 5. Hematoma volume and estimated number of macrophages in 5 dogs

	Hematoma volume (mL)					
Dog	12 h	3 d	5 d	10 d	24 d	No. of macrophages
1	0.34	0.22	0.29	0.08	0.03	315
2	3.93	4.50	3.46	2.91	0.76	385
3	2.21	2.34	2.14	1.30	0.44	295
4	3.48	4.66	3.04	2.51	1.18	277
5	0.86	1.11	0.27	0.37	0.25	263
Mean ± 1 SD	2.16 ± 1.57	2.56 ± 1.99	1.84 ± 1.50	1.44 ± 1.26	0.53 ± 0.45	307 ± 48

Histopathology. The prominent hemorrhagic lesions were indicated by cavitary lesions containing numerous macrophages and extravasated erythrocytes in the white matter of the parietal lobe (Figure 5 A). The mean number of macrophages was 307 ± 48, and the values for individual experimented dogs are summarized in Table 5. Because macrophages phagocyte and degrade extravasated erythrocytes in hemorrhagic areas, these cells frequently contained hemosiderin. In this study, Prussian blue staining demonstrated hemosiderin-containing macrophages in discrete lesions of the white matter (Figure 5 B), but the cortex did not appear to be affected.

Discussion

The present study showed that the MRI characteristics of ICH in dogs vary over time. The temporal changes in the T1, T2, and GRE SI corresponded well with the human data,[4] with the exception of T2 and GRE hyperintensity at the early subacute stage in dogs. In addition, the ADC value of the hemorrhagic lesions in dogs was increased at the same stage. The DWI SIR was positively correlated with the T2 and GRE SIR at the early subacute, late subacute, and chronic stages in dogs.

In clinical studies of human ICH, precisely ascertaining the interval between hemorrhage and MR imaging is frequently impossible and thus hampers efforts to investigate the processes in hemorrhagic stroke and develop possible treatments. Evaluating the underlying mechanisms of ICH-induced neuronal injury is similarly difficult in veterinary medicine. In addition, homogenous experimental groups of survivors of ICH for well-organized analysis, including histology, cannot be created during clinical studies. To overcome these limitations, we used an experimental model of ICH in dogs.

Currently, 3 modes of injection are used to induce ICH in animal models: balloon inflation, blood injection, and bacterial collagenase injection.[16] Among these, collagenase injection is the preferred method because it mimics the physiologic conditions of hematoma expansion observed in clinical patients with ICH.[16] In the present study, the MR features of hematomas varied little among the study dogs. This finding demonstrates the appropriateness of collagenase injection for obtaining reproducible results in the study of canine ICH.

The MRI characteristics of hemorrhage vary depending on both the chemical state and the integrity of the RBC membrane.[11] The electrons of outer orbital determine the magnetic properties

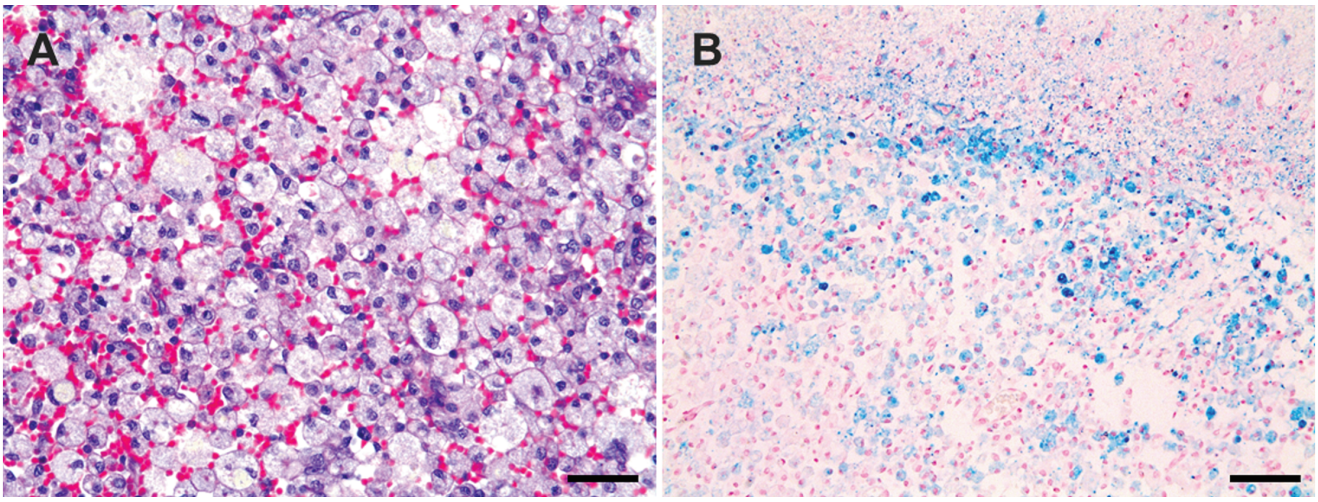

Figure 5. Microscopic features of the canine brain after experimentally induced ICH. (A) Cavitated areas containing numerous macrophages and extravasated erythrocytes were identified in the white matter of the parietal lobe. Hematoxylin and eosin stain; magnification, 400×; Scale bar, 35 µm. (B) Prussian blue stain was found in macrophages, which were distributed among discrete lesions of white matter. Magnification, 200×; Scale bar, 70 µm.

(diamagnetic or paramagnetic) of the iron in hemoglobin. Unpaired electrons alter the T1 and T2 relaxation times of water protons through magnetic dipole–dipole interactions and susceptibility effects. Dipole–dipole interactions shorten both the T1 and T2 relaxation times, but the effect is pronounced on T1WI. Compartmentalization of iron within the RBC membrane causes inhomogeneity in the magnetic field (the 'magnetic susceptibility effect') and thus shortens T2 without affecting T1. When the RBC membrane degrades, the susceptibility effect disappears, the T2 relaxation process is lost, and the signal on T2WI brightens.[4] In the present study, the T1 SI in dogs was similar to that in humans and reflected the evolution of ICH. This similarity was maintained for the T2 and GRE sequences, except for the early subacute stage (humans, hypointense; dogs, hyperintense). Because homogeneously distributed iron (loss of susceptibility effect) after RBC lysis induces signal hyperintensity on T2 and GRE sequences, degradation of the RBC membranes in canine ICH may begin to occur at early subacute stage, at least 5 d after the induction of hemorrhage, instead of late the subacute stage, as in humans. In comparison, the time course of ICH stages is much faster in rats—hyperacute at 0 to 6 h after induction, acute and early subacute stages at 24 to 72 h, and chronic stage at 7 d—than in humans and dogs:.[3] Together, these findings suggest that the rate of RBC degradation may differ between species.

In animal models of ICH, perihematomal edema peaks approximately 3 or 4 d after hemorrhage and then decreases slowly over time.[9,25,29,30] Among the several phases of edema formation after ICH, the late phase is associated with RBC lysis and hemoglobin toxicity.[26] The disruption of the blood–brain barrier contributes to the formation of posthemorrhage edema as well.[30] Therefore, both vasogenic edema as well as erythrocyte degradation may influence the T2 hyperintensity observed during the early subacute stage.

DWI measures the restricted motion of water molecules from the intracellular space in brain.[13] ADC trace maps are calculated from DWI images and are more sensitive to water diffusion in brain tissue than is DWI.[13] A previous human study showed that early hematomas containing intact RBC membranes yielded low ADC values, which increased after RBC lysis.[1] Because the hematomas in dogs instead had increased ADC measurements at the early subacute stage, RBC lysis might occur during this period. This finding supports the suspected relationship between the hyperintensities on T2 and GRE imaging and RBC lysis during the early subacute stage of canine ICH.

In addition to the restriction of diffusion, the T2 SI level may play an important role in the DWI SI.[20] The term 'T2 shine-through' describes the substantial contribution of T2 hyperintensity observed on DWI. In contrast, the correlation between T2 and DWI hypointensity is known as the 'T2 blackout effect.' First studied in ischemic stroke, this effect has since been investigated in a wide range of brain diseases.[22] T2 and DWI SI show strong correlation in human hematomas.[20] Similarly, DWI SI was positively correlated with T2 and GRE SI in dogs. In addition, T2 and DWI both yielded hyperintensities during the early subacute stage and hypointensities during the chronic stage. Therefore, T2 shine-through occurred at the early subacute stage, whereas the T2 blackout effect was noted at the chronic stage in canine ICH.

In conclusion, MRI is an ideal method for characterizing the temporal evolution of parenchymal alterations after ICH in dogs as well as in humans. Unlike in the theoretical MRI appearance of ICH, early subacute hemorrhagic lesions were hyperintense on T2WI and GRE images. DWI-SI was positively correlated with T2- and GRE-SI from the early subacute stage on. The present data might be useful for differentiating the clinical stages of ICH in dogs.

Acknowledgment

This research was supported by a Basic Science Research Program through the National Research Foundation of Korea (NRF) funded by the Ministry of Science, ICT, and Future Planning (NRF-2014R1A1A1036387).

References

1. **Atlas SW, DuBois P, Singer MB, Lu D.** 2000. Diffusion measurements in intracranial hematomas: implications for MR imaging of acute stroke. Am J Neuroradiol **21:**1190–1194.
2. **Barkovich AJ, Atlas SW.** 1988. Magnetic resonance imaging of intracranial hemorrhage. Radiol Clin North Am **26:**801–820.

3. **Belayev L, Obenaus A, Zhao W, Saul I, Busto R, Wu C, Vigdorchik A, Lin B, Ginsberg MD.** 2007. Experimental intracerebral hematoma in the rat: characterization by sequential magnetic resonance imaging, behavior, and histopathology. Effect of albumin therapy. Brain Res **1157:**146–155.
4. **Bradley WG Jr.** 1993. MR appearance of hemorrhage in the brain. Radiology **189:**15–26.
5. **Broderick J, Connolly S, Feldmann E, Hanley D, Kase C, Krieger D, Mayberg M, Morgenstern L, Ogilvy CS, Vespa P, Zuccarello M, American Heart Association, American Stroke Association Stroke Council, High Blood Pressure Research Council, Quality of Care and Outcomes in Research Interdisciplinary Working Group**. 2007. Guidelines for the management of spontaneous intracerebral hemorrhage in adults, 2007 update: a guideline from the American Heart Association/American Stroke Association Stroke Council, High Blood Pressure Research Council, and the Quality of Care and Outcomes in Research Interdisciplinary Working Group. Stroke **38:**2001–2023.
6. **Brooks RA, Di Chiro G, Patronas N.** 1989. MR imaging of cerebral hematomas at different field strengths: theory and applications. J Comput Assist Tomogr **13:**194–206.
7. **Carhuapoma JR, Wang PY, Beauchamp NJ, Keyl PM, Hanley DF, Barker PB.** 2000. Diffusion-weighted MRI and proton MR spectroscopic imaging in the study of secondary neuronal injury after intracerebral hemorrhage. Stroke **31:**726–732.
8. **Del Bigio MR, Yan HJ, Buist R, Peeling J.** 1996. Experimental intracerebral hemorrhage in rats magnetic resonance imaging and histopathological correlates. Stroke **27:**2312–2319.
9. **Enzmann DR, Britt RH, Lyons BE, Buxton JL, Wilson DA.** 1981. Natural history of experimental intracerebral hemorrhage: sonography, computed tomography and neuropathology. Am J Neuroradiol **2:**517–526.
10. **Feigin VL, Lawes CM, Bennett DA, Barker-Collo SL, Parag V.** 2009. Worldwide stroke incidence and early case fatality reported in 56 population-based studies: a systematic review. Lancet Neurol **8:**355–369.
11. **Gomori JM, Grossman RI, Goldberg HI, Zimmerman RA, Bilaniuk LT.** 1985. Intracranial hematomas: imaging by high-field MR. Radiology **157:**87–93.
12. **Gomori JM, Grossman RI, Yu-Ip C, Asakura T.** 1987. NMR relaxation times of blood: dependence on field strength, oxidation state, and cell integrity. J Comput Assist Tomogr **11:**684–690.
13. **Hillock SM, Dewey CW, Stefanacci JD, Fondacaro JV.** 2006. Vascular encephalopathies in dogs: diagnosis, treatment, and prognosis. Compend Contin Educ Vet **28:**208–217.
14. **Kang BT, Lee JH, Jung DI, Park C, Gu SH, Jeon HW, Jang DP, Lim CY, Quan FS, Kim YB, Cho ZH, Woo EJ, Park HM.** 2007. Canine model of ischemic stroke with permanent middle cerebral artery occlusion: clinical and histopathological findings. J Vet Sci **8:**369–376.
15. **Kirkman MA, Allan SM, Parry-Jones AR.** 2011. Experimental intracerebral hemorrhage: avoiding pitfalls in translational research. J Cereb Blood Flow Metab **31:**2135–2151.
16. **Ma Q, Khatibi NH, Chen H, Tang J, Zhang JH.** 2011. History of preclinical models of intracerebral hemorrhage. Acta Neurochir Suppl **111:**3–8.
17. **Parizel PM, Makkat S, Van Miert E, Van Goethem J, van den Hauwe L, De Schepper AM.** 2001. Intracranial hemorrhage: principles of CT and MRI interpretation. Eur Radiol **11:**1770–1783.
18. **Rink C, Christoforidis G, Abduljalil A, Kontzialis M, Bergdall V, Roy S, Khanna S, Slivka A, Knopp M, Sen CK.** 2008. Minimally invasive neuroradiologic model of preclinical transient middle cerebral artery occlusion in canines. Proc Natl Acad Sci USA **105:**14100–14105.
19. **Saver JL, Albers GW, Dunn B, Johnston KC, Fisher M,** STAIR VI Consortium. 2009. Stroke Therapy Academic Industry Roundtable (STAIR) recommendations for extended-window acute stroke therapy trials. Stroke **40:**2594–2600.
20. **Silvera S, Oppenheim C, Touzé E, Ducreux D, Page P, Domigo V, Mas JL, Roux FX, Fredy D, Meder JF.** 2005. Spontaneous intracerebral hematoma on diffusion-weighted images: influence of T2-shine-through and T2-blackout effects. Am J Neuroradiol **26:**236–241.
21. **Schellinger PD, Jansen O, Fiebach JB, Hacke W, Sartor K.** 1999. A standardized MRI stroke protocol comparison with CT in hyperacute intracerebral hemorrhage. Stroke **30:**765–768.
22. **Stadnik TW, Demaerel P, Luypaert RR, Chaskis C, Van Rompaey KL, Michotte A, Osteaux MJ.** 2003. Imaging tutorial: differential diagnosis of bright lesions on diffusion-weighted MR images. Radiographics **23:**e7.
23. **Tamura S, Tamura Y, Tsuka T, Uchida K.** 2006. Sequential magnetic resonance imaging of an intracranial hematoma in a dog. Vet Radiol Ultrasound **47:**142–144.
24. **Thulborn KR, Brady TJ.** 1989. Iron in magnetic resonance imaging of cerebral hemorrhage. Magn Reson Q **5:**23–38.
25. **Tomita H, Ito U, Ohno K, Hirakawa K.** 1994. Chronological changes in brain edema induced by experimental intracerebral hematoma in cats. Acta Neurochir Suppl (Wien) **60:**558–560.
26. **Wagner KR, Xi G, Hua Y, Kleinholz M, de Courten-Myers GM, Myers RE, Broderick JP, Brott TG.** 1996. Lobar intracerebral hemorrhage model in pigs: rapid edema development in perihematomal white matter. Stroke **27:**490–497.
27. **Weingarten K, Zimmerman RD, Deo-Narine V, Markisz J, Cahill PT, Deck MD.** 1991. MR imaging of acute intracranial hemorrhage: findings on sequential spin-echo and gradient-echo images in a dog model. Am J Neuroradiol **12:**457–467.
28. **Wessmann A, Chandler K, Garosi L.** 2009. Ischaemic and haemorrhagic stroke in the dog. Vet J **180:**290–303.
29. **Xi G, Keep RF, Hoff JT.** 1998. Erythrocytes and delayed brain edema formation following intracerebral hemorrhage in rats. J Neurosurg **89:**991–996.
30. **Yang GY, Betz AL, Chenevert TL, Brunberg JA, Hoff JT.** 1994. Experimental intracerebral hemorrhage: relationship between brain edema, blood flow, and blood–brain barrier permeability in rats. J Neurosurg **81:**93–102.